C. R. Mecanique 343 (2015) 589–598

Contents lists available at ScienceDirect

Comptes Rendus Mecanique

www.sciencedirect.com

Discrete simulation of fluid dynamics

Finite-difference lattice Boltzmann simulation on acoustics-induced particle deposition

Sau-Chung Fu [a,b,*], Wai-Tung Yuen [a], Chili Wu [b], Christopher Yu-Hang Chao [a]

[a] Department of Mechanical and Aerospace Engineering, The Hong Kong University of Science and Technology, Hong Kong, China
[b] Building Energy Research Center, Fok Ying Tung Graduate School, The Hong Kong University of Science and Technology, Hong Kong, China

ARTICLE INFO

Article history:
Received 2 December 2014
Accepted 29 July 2015
Available online 10 August 2015

Keywords:
Finite difference method
Lattice Boltzmann method
Acoustic streaming
Acoustic radiation pressure
Particle deposition
Filtration

ABSTRACT

Particle manipulation by acoustics has been investigated for many years. By a proper design, particle deposition can be induced by the same principle. The use of acoustics can potentially be developed into an energy-efficient technique for particle removal or filtration system as the pressure drop due to acoustic effects is low and the flow velocity is not necessary to be high. Two nonlinear acoustic effects, acoustic streaming and acoustic radiation pressure, are important. Acoustic streaming introduces vortices and stagnation points on the surface of an air duct and removes the particles by deposition. Acoustic radiation pressure causes particles to form agglomerates and enhances inertial impaction and/or gravitational sedimentation. The objective of this paper is to develop a numerical model to investigate the particle deposition induced by acoustic effects. A three-step approach is adopted and lattice Boltzamnn technique is employed as the numerical method. This is because the lattice Boltzmann equation is hyperbolic and can be solved locally, explicitly, and efficiently on parallel computers. In the first step, the acoustic field and its mean square fluctuation values are calculated. Due to the advantage of the lattice Boltzmann technique, a simple, stable and fast lattice Boltzmann method is proposed and verified. The result of the first step is input into the second step to solve for acoustic streaming. Another finite difference lattice Boltzmann method, which has been validated by a number of flows and benchmark cases in the literature, is used. The third step consists in tracking the particle's motion by a Lagrangian approach where the acoustic radiation pressure is considered. The influence of the acoustics effects on particle deposition is explained. The numerical result matches with an experiment. The model is a useful tool for optimizing the design and helps to further develop the technique.

1. Introduction

In most of the filtration and aerosol removal systems, particles are removed from the main air stream by deposition. For example, separators such as cyclones use external centripetal forces to displace particles from the main air stream, which are collected by deposition due to inertial impaction. In a filter, fibers introduce sudden changes in the airflow velocity and the particles are deposited onto them by interception and impaction. In these systems, either a high airflow velocity

* Corresponding author at: Department of Mechanical and Aerospace Engineering, The Hong Kong University of Science and Technology, Hong Kong, China.
E-mail address: mescfu@ust.hk (S.C. Fu).

http://dx.doi.org/10.1016/j.crme.2015.07.012
1631-0721/

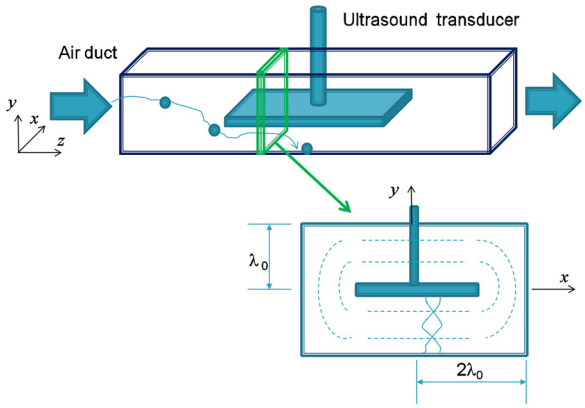

Fig. 1. (Color online.) Schematic diagram of the proposed filtration system.

is used or a high-pressure drop is required to be overcome, resulting in high energy consumption [1–3]. Recently, by using nonlinear acoustic effects, an innovative aerosol removal technique without high-pressure drop or high airflow velocity has been proposed, which has the potential to be developed into an energy efficient aerosol removal technique [4].

In the experiment carried out in [4], an ultrasonic transducer that generated an acoustic field was installed in an air duct. Particles were deposited and removed from the air stream by deposition onto the wall of the channel when passing through the air duct. By defining the removal efficiency as the number of particles removed with and without acoustic effects, the experiment shows that the removal efficiency increases by 20–30% by turning on the ultrasound transducer. Two nonlinear acoustic effects—acoustic streaming and acoustic radiation pressure—were studied and were accountable for the enhancement of the deposition. Acoustic streaming [5,6] causes vortices and enhances inertial impaction. Acoustic radiation pressure enhances deposition and sedimentation by encouraging particles to agglomerate and grow in size [7–9]. Although the experimental results give evidences to support the contributions of the two nonlinear effects, details of the flow and the particle dynamics are complicated in the acoustic field and cannot be revealed due to the limited precision of the existing experimental techniques. It is desirable to develop a mathematical model to further study the physics behind. A successful model also helps to optimize the design, so that an energy-efficient filtration technique can be developed.

Lattice Boltzmann method (LBM) has been developed into an alternative and a promising numerical scheme for the modeling of fluid physics and simulating fluid flows [10–12]. The equation is hyperbolic and can be solved locally, explicitly, and efficiently on parallel computers. Many versions of LBM have been developed for being applied to different kinds of flows with varying degrees of success. Recently, the finite-difference lattice Boltzmann method (FDLBM) proposed and developed by Fu et al. [13] provides a convenient algorithm for setting the boundary condition. Also, it eliminates the inherent compressibility effect of the conventional LBM [14]. The method is capable of simulating a number of flows including microchannel flow [13], stochastic flow [15], thermal incompressible flows [16], blood flow with complex boundary [17], natural convection with magnetic field effect [18], double diffusive mixed convection [19] and non-Newtonian flows [17–19].

The objective of this paper is to develop a numerical model to investigate particle deposition induced by acoustic effects in a duct flow. Since the study involves particle dynamics and two acoustic effects that are nonlinear and second order, a three-step approach is employed. Firstly, the acoustic field is found by solving the linear wave equations. A new LBM for the wave equations is proposed and verified. By using the mean square values of the acoustic field, acoustic streaming is determined in step two. The numerical method employed in this second step is the FDLBM by [13]. The ability of the FDLBM in applying to acoustic streaming is also demonstrated. After obtaining the flow pattern, the trajectory of a large number of particles are traced by a Lagrangian approach in step three. The acoustic radiation pressure is incorporated into the force balance equation of the particle dynamics.

2. Methodology

The schematic diagram of the proposed filtration system is shown in Fig. 1. It is essentially an air duct installed with an ultrasound transducer. The frequency of the ultrasound is 30 kHz and the wavelength (λ_0) is 0.011 m. The height (y-direction) of the duct is $2\lambda_0$ and the width (x-direction) of the duct is $4\lambda_0$. In this setting, standing waves with two pressure nodes between the transducer and the channel wall together with complicated sound field at the edge of the transducer are generated. Due to the acoustic effects, the particles entering the duct are encouraged to deposit onto the walls of the channel. The region affected by the ultrasound is assumed to be long, so that it is adequate to carry out a 2-dimensional simulation in x–y plane. The duration of particles in the region is the length (z-direction) of the transducer (20 cm) divided by the air flow velocity (0.2 m/s) and it is about 1 s.

Since the two acoustic effects are second-order effects, the simulation is divided into three steps. Firstly, the linear wave equations are solved to find the mean square fluctuations of the sound field. By using the mean square values of the sound

Table 1
List of input parameters.

Parameter	Symbol	Value
Density of air	ρ_0	1.206 kg/m^3
Temperature of air	T_0	273 K
Atmospheric pressure	P_0	131333.4 Pa
Speed of sound in air	c_0	330 m/s
Viscosity of air	μ	1.8·e^{-5} Pa·s
Acoustic wave frequency	*freq*	30000 Hz
Acoustic wave length	λ_0	0.011 m
Particle density	ρ_p	1050 kg/m^3
Speed of sound in particle	c_p	1479 m/s

field, the flow field due to acoustic streaming is determined by solving the incompressible Navier–Stokes (NS) equation. The last step is to trace the particle motion including the effect of the acoustic radiation pressure by a Lagrangian approach, so that the influence of the acoustic effects on particle deposition is investigated.

2.1. Acoustic wave

In the first step, the following normalization is employed. The length (x, y) is normalized by the wavelength of the ultrasound, and the time (t) is normalized by the period of the ultrasound. Due to symmetry, only a quadrant of the physical domain is calculated (i.e. $0 \le \tilde{x} \le 2$ and $0 \le \tilde{y} \le 1$; here and after, the symbol with a 'tilde' is dimensionless and that without a 'tilde' is dimensional), where the ultrasound transducer is located at $\tilde{y} = 0$ and $0 \le \tilde{x} \le 1$. It is supposed that the transducer generates a sinusoidal pressure fluctuation with an amplitude (A_0) of 1788.86 Pa, which corresponds to a sound pressure level of 156 dB. The fluctuating pressure (p') is normalized by its amplitude. The fluctuating density (ρ') is normalized by A_0/c_0^2 where $c_0 = 330$ m/s is the speed of sound in air. In this normalization, $\tilde{p}' = \tilde{\rho}'$. The fluctuating velocity (u', v') is normalized by $U_1 = A_0/c_0\rho_0 = 4.49$ m/s where ρ_0 is the density of air. A summary of the input parameters can be found in Table 1.

The normalized governing equations (linear wave equations) are

$$\frac{\partial \tilde{\rho}'}{\partial \tilde{t}} + \frac{\partial \tilde{u}'}{\partial \tilde{x}} + \frac{\partial \tilde{v}'}{\partial \tilde{y}} = 0 \tag{1}$$

$$\frac{\partial \tilde{u}'}{\partial \tilde{t}} + \frac{\partial \tilde{\rho}'}{\partial \tilde{x}} = 0 \tag{2}$$

$$\frac{\partial \tilde{v}'}{\partial \tilde{t}} + \frac{\partial \tilde{\rho}'}{\partial \tilde{y}} = 0 \tag{3}$$

The boundary condition at the transducer is $\tilde{p}' = \sin(2\pi\tilde{t})$, slip and impermeable conditions are applied at the walls ($\tilde{x} = 2$ or $\tilde{y} = 1$), and the remaining sides ($\tilde{x} = 0$ or $\tilde{y} = 0$) are reflective boundary conditions.

Due to the advantage of LBM, a new LBM, which is stable and simple for the wave equations, is proposed. The lattice velocities are defined as

$$\tilde{\xi}_0 = (0,0), \quad \tilde{\xi}_1 = (\tilde{c},0), \quad \tilde{\xi}_2 = (0,\tilde{c}), \quad \tilde{\xi}_3 = (-\tilde{c},0), \quad \tilde{\xi}_4 = (0,-\tilde{c}) \tag{4}$$

where $\tilde{c} = \Delta\tilde{x}/\Delta\tilde{t}$ is a scaling parameter and $\Delta\tilde{x}$ and $\Delta\tilde{t}$ are the grid size and the size of the time step, respectively. To solve the wave equations, Eqs. (1)–(3), it is equivalent to solve

$$\tilde{f}_\alpha^{eq}(\tilde{t} + \Delta\tilde{t}, \hat{x}) = \tilde{f}_\alpha^{eq}(\tilde{t}, \hat{x} - \tilde{\xi}_\alpha \Delta\tilde{t}) \tag{5}$$

where $\tilde{f}_\alpha^{eq}$ is the discrete particle distribution function, $\hat{x} = (\tilde{x}, \tilde{y})$ and $\tilde{\xi}_\alpha = (\tilde{\xi}_{\alpha x}, \tilde{\xi}_{\alpha y})$ with index $\alpha = 0..4$. By fulfilling the constraints,

$$\begin{aligned}
\Sigma \tilde{f}_\alpha^{eq} &= \tilde{\rho}' \\
\Sigma \tilde{f}_\alpha^{eq} \tilde{\xi}_{\alpha x} &= \tilde{u}' \\
\Sigma \tilde{f}_\alpha^{eq} \tilde{\xi}_{\alpha y} &= \tilde{v}' \\
\Sigma \tilde{f}_\alpha^{eq} \tilde{\xi}_{\alpha x}^2 = \Sigma \tilde{f}_\alpha^{eq} \tilde{\xi}_{\alpha y}^2 &= \tilde{\rho}' \\
\Sigma \tilde{f}_\alpha^{eq} \tilde{\xi}_{\alpha x} \tilde{\xi}_{\alpha y} &= 0
\end{aligned} \tag{6}$$

the discrete particle distribution function can be obtained as

$$\tilde{f}_\alpha^{eq} = \tilde{\rho}'(A_\alpha + A_{\alpha x}\tilde{\xi}_{\alpha x}\tilde{u}' + A_{\alpha y}\tilde{\xi}_{\alpha y}\tilde{v}') \tag{7}$$

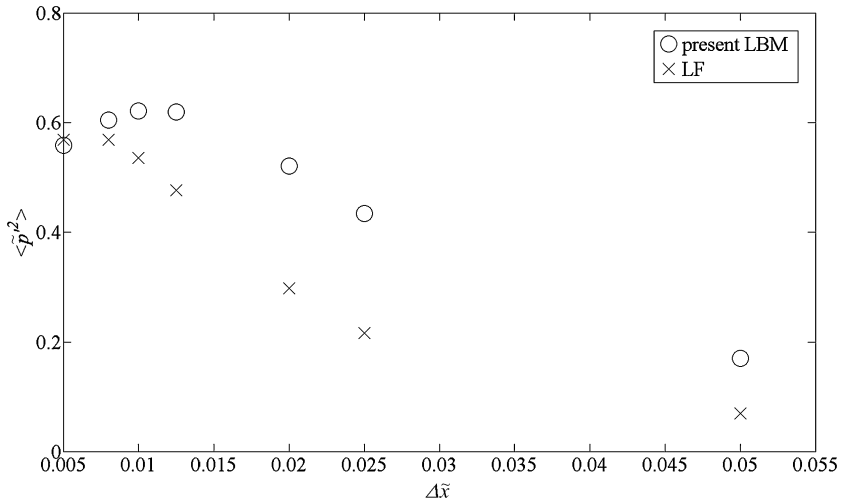

Fig. 2. Grid analysis and comparison of the present LBM to Lax–Friedrichs' method ($\Delta\tilde{x} = \Delta\tilde{y}, \tilde{c} = \Delta\tilde{x}/\Delta\tilde{t} = 2$).

where

$$
\begin{aligned}
&A_0 = \frac{\tilde{c}^2 - 2}{\tilde{c}^2}, \quad A_1 = A_2 = \frac{1}{2\tilde{c}^2} \\
&A_{1x} = A_{2y} = \frac{1}{2\tilde{\rho}'\tilde{c}^2}, \quad A_{2x} = A_{1y} = 0 \\
&A_3 = A_1, \quad A_4 = A_2 \\
&A_{3x} = A_{1x}, \quad A_{4x} = A_{2x} \\
&A_{3y} = A_{1y}, \quad A_{4y} = A_{2y}
\end{aligned} \tag{8}
$$

The mean square fluctuations ($< \cdot >$) of the acoustic field are found by taking summation of the quantities over a wave period of time. The interested mean square values are $< p'^2 >$, $< u'^2 >$, $< v'^2 >$ and $< u'v' >$. The calculation continues until steady mean-square values are obtained (with absolute error less than 1·e–5). A grid analysis was carried out for $< p'^2 >$ at the position $\tilde{x} = 2, \tilde{y} = 0$ (Fig. 2). The result calculated by the present LBM agrees with that calculated by Lax–Friedrichs method [24], thus the proposed LBM is verified. Hence, the results from this step is reliable and can be utilized in the next step.

2.2. Acoustic streaming

The non-zero mean square fluctuations of the acoustic field are the driving forces for acoustic streaming, represented by the nonlinear terms in the NS equations. This is a second-order effect, but due to the high frequency of the ultrasound, the time scale becomes significant when compared to the airflow. In this step, the steady incompressible NS equations are solved with the acoustic statistics as inputs as body force terms. The characteristic velocity is chosen to be $U_s = U_1^2/c_0$ which is the peak streaming velocity obtained by Rayleigh [20] in the mid-plane of the channel for standing waves in wide channels. The pressure p is normalized by $\rho_0 U_s^2$. The normalized governing equations are

$$\frac{\partial\tilde{u}}{\partial\tilde{x}} + \frac{\partial\tilde{v}}{\partial\tilde{y}} = 0 \tag{9}$$

$$\tilde{u}\frac{\partial\tilde{u}}{\partial\tilde{x}} + \tilde{v}\frac{\partial\tilde{u}}{\partial\tilde{y}} = -\frac{\partial\tilde{p}}{\partial\tilde{x}} + \frac{1}{Re}\left(\frac{\partial^2}{\partial\tilde{x}^2} + \frac{\partial^2}{\partial\tilde{y}^2}\right)\tilde{u} - S\left(\frac{\partial < \tilde{u}'^2 >}{\partial\tilde{x}} + \frac{\partial < \tilde{u}'\tilde{v}' >}{\partial\tilde{y}}\right) \tag{10}$$

$$\tilde{u}\frac{\partial\tilde{v}}{\partial\tilde{x}} + \tilde{v}\frac{\partial\tilde{v}}{\partial\tilde{y}} = -\frac{\partial\tilde{p}}{\partial\tilde{y}} + \frac{1}{Re}\left(\frac{\partial^2}{\partial\tilde{x}^2} + \frac{\partial^2}{\partial\tilde{y}^2}\right)\tilde{v} - S\left(\frac{\partial < \tilde{u}'\tilde{v}' >}{\partial\tilde{x}} + \frac{\partial < \tilde{v}'^2 >}{\partial\tilde{y}}\right) \tag{11}$$

where $S = U_1^2/U_s^2 = 5401.76$ is due to the different velocity scalings between the first- and second-order equations, Re is the Reynolds number and, in this case, its value is 44.84. Again, only a quadrant of the physical domain is calculated (i.e. $0 \le \tilde{x} \le 2$ and $0 \le \tilde{y} \le 1$). For the boundary condition, no slip is applied on the wall. Symmetric boundary conditions are used on the left and on the bottom, including the position of the transducer. The equations are solved by FDLBM [13]. The details of the numerical method can be found in [13] and are not repeated here. The numerical parameters are $\Delta\tilde{x} = \Delta\tilde{y} = 0.01$ and $\Delta\tilde{t} = 1{\cdot}e{-}5$.

2.3. Particle dynamics

In this step, the particles dynamics due to acoustic effects are simulated. It is assumed that the particles have the same properties as water, without evaporation effects. A large number of particles with initial diameter of 6 μm are randomly distributed in the domain. The motion of the particles is governed by [21,22]:

$$\frac{\mathrm{d}\bar{x}_\mathrm{p}}{\mathrm{d}t} = \bar{u}_\mathrm{p} \tag{12}$$

$$\frac{\mathrm{d}\bar{u}_\mathrm{p}}{\mathrm{d}t} = \frac{f_D}{\tau_\mathrm{p}}\left(\bar{u} - \bar{u}_\mathrm{p}\right) + \bar{F}_\mathrm{p} \tag{13}$$

where $\bar{x}_\mathrm{p}$ is the location of the particle, $\bar{u}_\mathrm{p}$ is the velocity of the particle, $\bar{u} = (u, v)$ is the flow velocity, which is obtained in the previous step, f_D is the Stoke's drag modification function. For the particle's Reynolds number, $Re_\mathrm{p} = \rho_\mathrm{p}|\bar{u} - \bar{u}_\mathrm{p}|\,\mathrm{d}_\mathrm{p}/\mu < 800$, it can be estimated as

$$f_D(Re_\mathrm{p}) = 1 + 0.15Re_\mathrm{p}^{0.687} \tag{14}$$

The aerosol characteristic response time is defined as

$$\tau_\mathrm{p} = \frac{\rho_\mathrm{p}\mathrm{d}_\mathrm{p}^2 C_\mathrm{c}}{18\mu} \tag{15}$$

where ρ_p is the particle density, d_p is the aerodynamic diameter of the particle, μ is the viscosity of air, and C_c is the Cunningham slip correction factor for small size aerosol,

$$C_\mathrm{c} = 1 + \frac{2\lambda}{\mathrm{d}_\mathrm{p}}\left[1.257 + 0.4\exp\left(-\frac{1.1\mathrm{d}_\mathrm{p}}{2\lambda}\right)\right] \tag{16}$$

The mean free path of air molecules (λ) is 6.8·e–8 m.

Apart from the drag forces, other external forces are also considered in Eq. (13), including gravity ($\bar{F}_\mathrm{g}$), Brownian motion ($\bar{F}_\mathrm{B}$) and acoustic radiation pressure ($\bar{F}_\mathrm{A}$), but the lift and the force due to thermophoresis are neglected. The force due to Brownian motion is evaluated at every time step by [23]

$$\bar{F}_\mathrm{B} = \bar{\zeta}\sqrt{\frac{\pi S_0}{\Delta t}} \tag{17}$$

where

$$S_0 = \frac{216\mu\sigma T}{\pi^2 \mathrm{d}_\mathrm{p}^5(\rho_\mathrm{p}/\rho_0)^2 C_\mathrm{c}} \tag{18}$$

$\sigma = 1.38\text{e–}23$ J/K is the Stefan–Boltzmann constant, $T = 273$ K is the temperature, and $\bar{\zeta}$ is a random vector sampled from Gaussian distribution for each time step. The acoustic radiation pressure is modeled by [8]

$$\bar{F}_\mathrm{A} = -\nabla V \tag{19}$$

where

$$V = \frac{3}{2}\frac{\rho_0}{\rho_\mathrm{p}}\left[\frac{< p'^2 >}{3\rho_0^2 c_0^2} f_1 - \frac{< u'^2 > + < v'^2 >}{2} f_2\right]$$

$$f_1 = 1 - \frac{c_0^2\rho_0}{c_\mathrm{p}^2\rho_\mathrm{p}}, \quad f_2 = \frac{2(\rho_\mathrm{p} - \rho_0)}{2\rho_\mathrm{p} + \rho_0} \tag{20}$$

and c_p is the speed of sound in the particles. It should be noted that the secondary sonic forces may become important if two particles become close together [25], but it is not simulated in the current model. The current approach is an approximation by modeling the acoustic radiation pressure by [8] and the drag only due to acoustic streaming, so the Basset memory terms are negligible.

The particle dynamics including the effect of acoustic radiation pressure are simulated by Lagrangian approach according to the following algorithm:

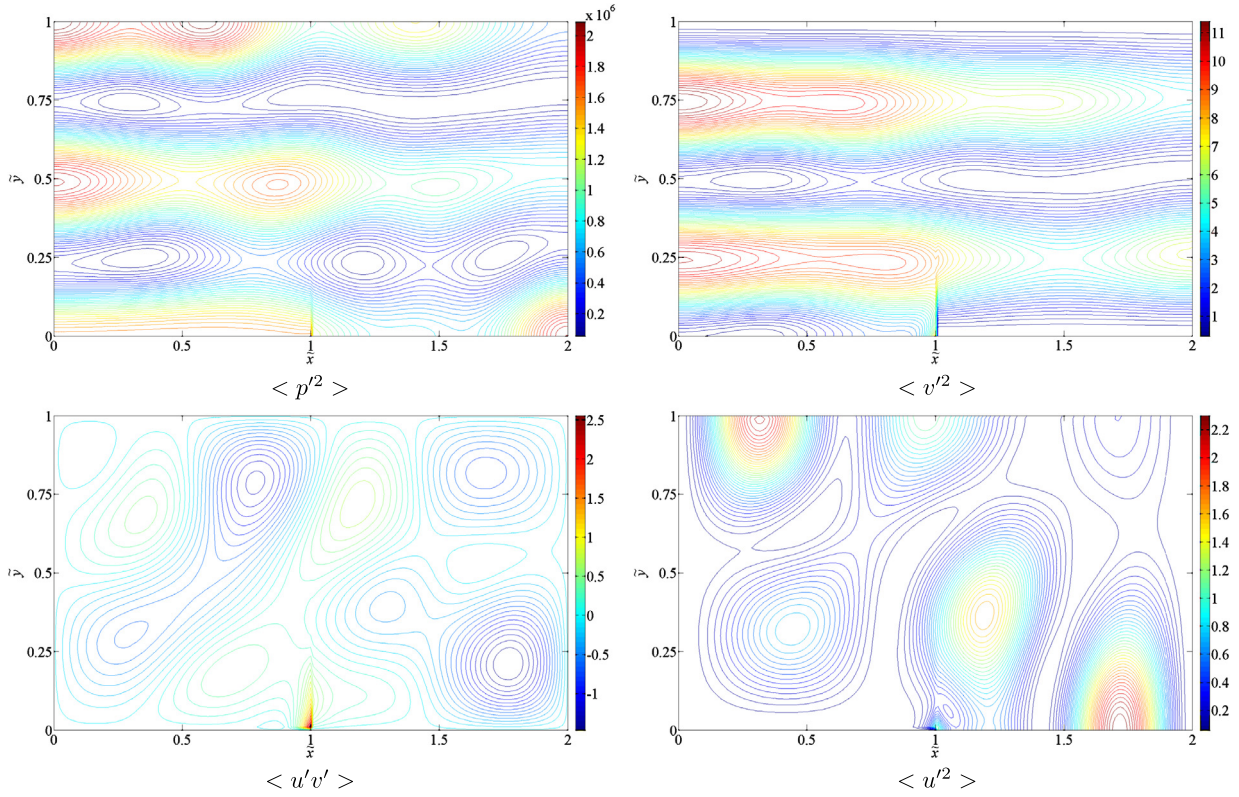

Fig. 3. (Color online.) Contours for mean square values of the acoustic field.

(i) a large number of particles ($N = 200$) are distributed in the computational domain randomly;
(ii) the locations of the particles are tracked according to Eq. (12). The velocities of the particles are calculated using Eq. (13). The differential equations are discretized by Euler's method (first-order forward-time finite difference method) explicitly. The size of the time step is $\Delta t = 1{\cdot}\text{e}{-}5$ s;
(iii) after a time step, the locations of all the particles are checked. If two particles are close to each other (at the distance less than the sum of their radius), they agglomerate and the size is redefined according to $\mathrm{d}p_{\text{new}} = (\mathrm{d}p_i^3 + \mathrm{d}p_j^3)^{-3}$, where the new agglomerate with diameter $\mathrm{d}p_{\text{new}}$ has the same volume as the sum of its daughter particles i and j;
(iv) if a particle is close to the wall, it is deposited (i.e. removed).

3. Results and discussions

In this section, the numerical results calculated by the method described in the previous section is presented. The acoustic field and the flow field due to acoustic streaming is analyzed. The motion of particles is investigated and the role of acoustic effects on the particle deposition is explained.

3.1. Result of acoustic wave

The contours of the mean square values of the acoustic field are plotted in Fig. 3. It is shown that a standing wave is generated at the middle of the ultrasound transducer along the y-axis and that two pressure nodes are observed. The location of the pressure nodes is the location of the (vertical) velocity anti-nodes. The magnitude of the vertical velocity is larger than that of the horizontal one. The standing wave is distorted where x is close to the edge of the transducer.

3.2. Result of acoustic streaming

The flow due to acoustic streaming is shown in Figs. 4 and 5. In Fig. 4, the contours of the dimensional velocities show that the magnitudes of the flow velocities can be up to 1 m/s. However, the horizontal velocity in most of the region is less than 0.5 m/s, except for the region close to the transducer, where a high-speed stream moves along and toward the middle of the transducer. Similarly, the vertical velocity in most of the region is less than 0.5 m/s, except for the region at the edge of the transducer, where a strong steam is present. It is clear from the vector plot (Fig. 5) that a number of vortices are developed by the acoustic streaming. It is noted that there are two stagnation points at the upper wall of the channel.

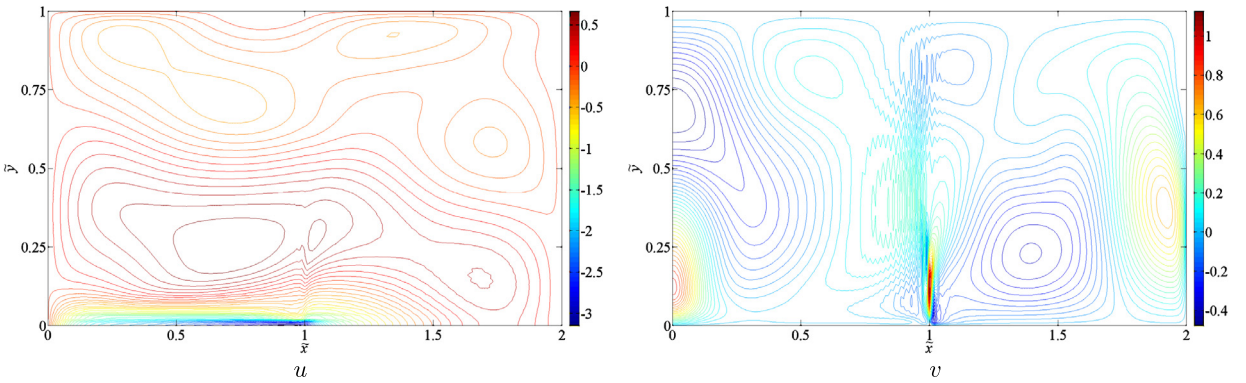

Fig. 4. (Color online.) Contours for acoustic streaming.

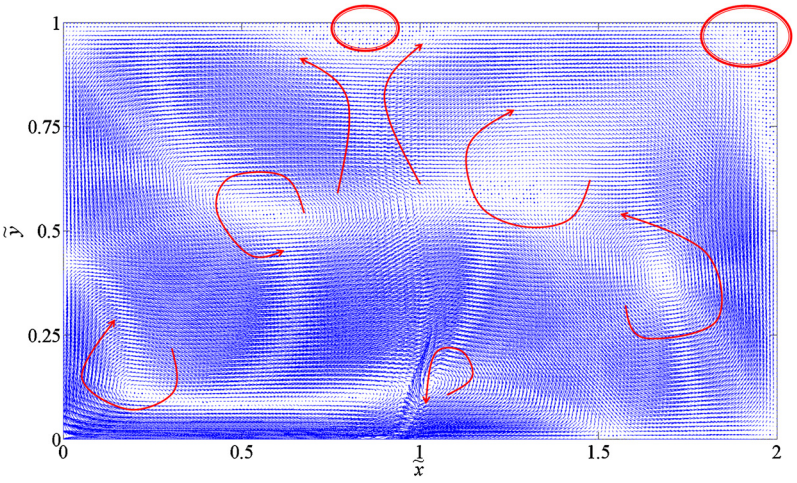

Fig. 5. (Color online.) Flow pattern for acoustic streaming.

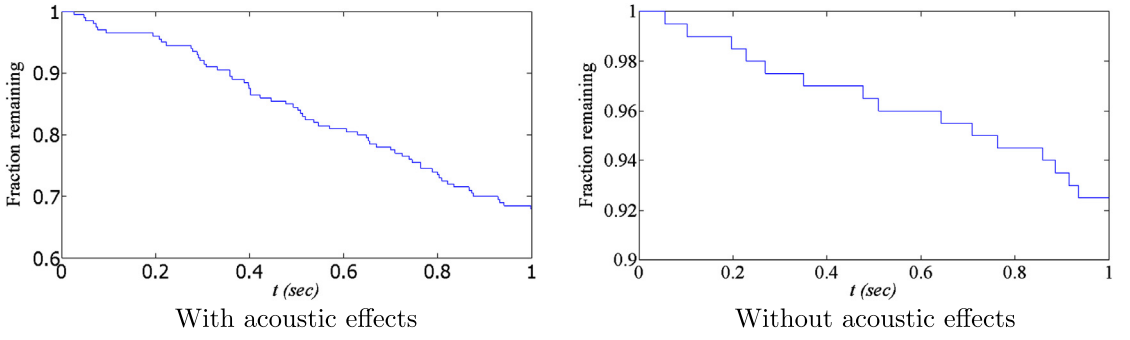

Fig. 6. (Color online.) Fraction of particles remaining against time.

3.3. Result of particle dynamics

In the third step of the modeling, motions of particles are tracked, and the duration of simulation is 1 s. It is observed that under the current temperature and particle size, the effect of the Brownian motion on particle deposition is not significant; this is consistent with the analysis by [25]. In Fig. 6, the fraction of particles remaining inside the domain is plotted against time. The figure, without acoustic effects, is the fraction simulated where the ultrasound transducer is turned off and there is no flow inside the domain. The deposition is solely due to gravitational sedimentation. The results show that, compared with the 30% particle deposition caused by acoustic effects, the deposition that occur without the acoustic effects is insignificant. The calculated removal efficiency affected by acoustics matches with the experimental result [4].

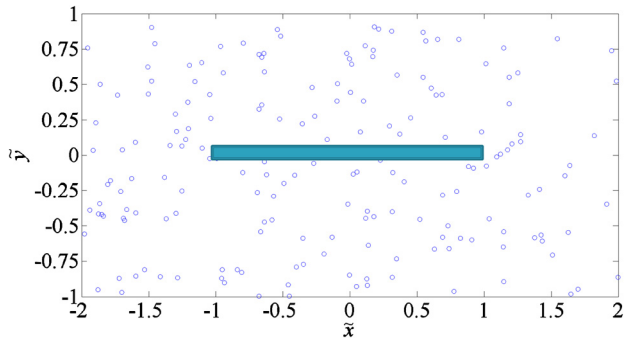

Fig. 7. (Color online.) Locations of particles after 1 s without acoustic effects.

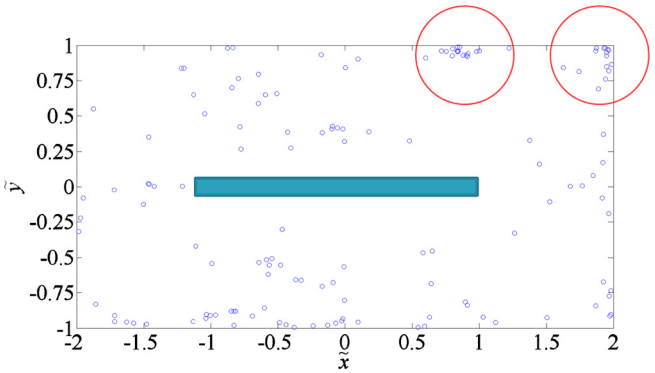

Fig. 8. (Color online.) Locations of particles after 1 s with acoustic effects.

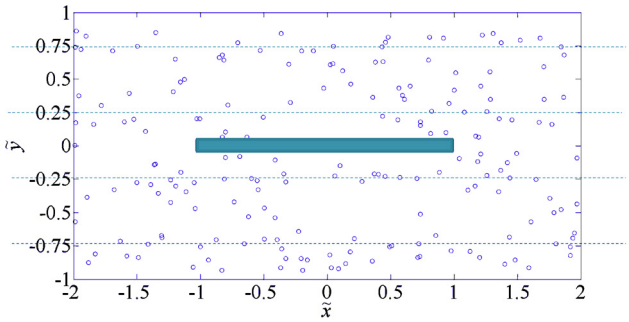

Fig. 9. (Color online.) Locations of particles after 1 s due to acoustic radiation pressure effect (without acoustic streaming).

In order to study the role of the acoustics on particle deposition, the positions of particles after 1 s in different scenarios are shown in Fig. 7 to 9. The rectangular box at the middle of the graph represents the ultrasound transducer. It was modeled to have zero thickness, but for the purpose of clear presentation, it is shown in the graph. In Fig. 7, no acoustic effects are applied. The deposition of particles is mainly due to gravity, and is minimal because the particle sizes are small. The particles are evenly and randomly distributed in the domain. In Fig. 8, particle deposition is clearly induced by acoustic effects. The particles are not evenly distributed in the domain, while particles agglomerate at some specific locations. For example, some particles agglomerate at the top right corner of the domain, as indicated by two circles in the figure. By comparing to the flow field (Fig. 5), it is noted that the indicated locations are the stagnation points of flow. It shows that the streaming carries particles to the wall and induces deposition. Since the initial size of particles is small, the effect of gravitational sedimentation should be minimal. However, more particles are found at the bottom of the channel. It is possible that the particles agglomerate and become larger by the vortices or by the acoustic radiation pressure, and enhance sedimentation.

To investigate the effect of acoustic radiation pressure, an idealized scenario with acoustic streaming being eliminated is shown in Fig. 9. The nodal positions of the pressure field are represented by the dotted lines. To further analyse the significance of acoustic radiation pressure, the vertical positions of different size particles (6 μm, 12 μm, and 24 μm) from three simulations are averaged and recorded. These results were obtained for times of 0.5 s. They are represented

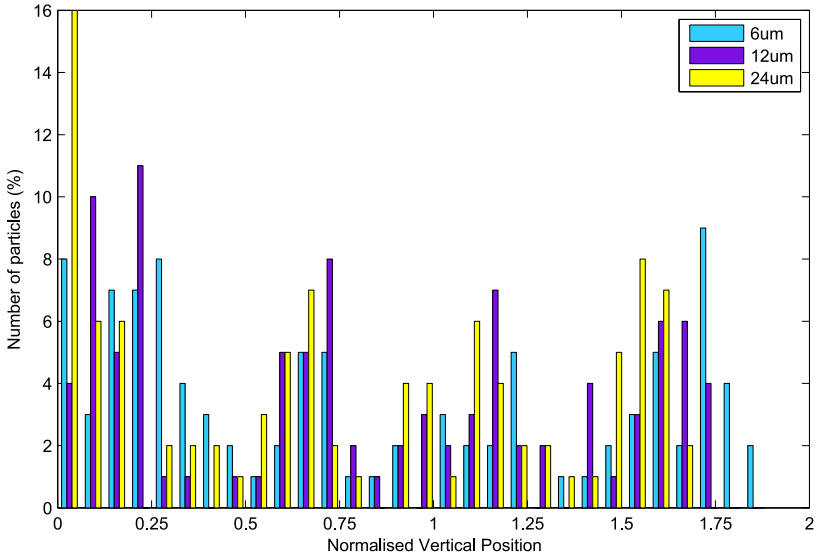

Fig. 10. (Color online.) Particles vertical position distribution after 0.5 second due to acoustic radiation pressure effect (without acoustic streaming).

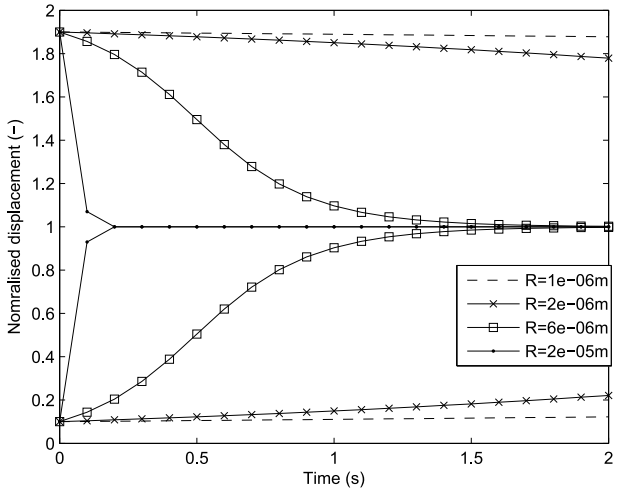

Fig. 11. Particle positions influenced by acoustic radiation and drag forces in a standing wave. (Distance normalized with a quarter of a wavelength, i.e. 0 and 2 are pressure antinodes and 1 is a pressure node.)

in a histogram in Fig. 10. The particles are found in positions near the pressure nodes, where the $\tilde{y}$-axes are 0.25, 0.75, 1.25 and 1.75. Although acoustic radiation forces on particles may be in the opposite direction to the gravitational force in some areas of the domain, Fig. 10 shows that the larger the particles are, the more concentrated they are on the bottom of the domain. This is especially significant for the 24 μm particles, found mostly between vertical positions $0 < \tilde{y} < 1$, and only 6 μm and 12 μm particles found between vertical positions $1.6 < \tilde{y} < 2$. Furthermore, as demonstrated by the particle positions influenced by acoustic radiation and drag forces in a pure standing wave in Fig. 11, the larger the particles were, the quicker they agglomerate towards the pressure nodes. Thus it can be concluded that while particles are small, acoustic streaming is the dominating agglomeration mechanism. However, as particle sizes are larger (either by input or agglomeration), acoustic radiation pressure becomes significant in the encouragement of agglomeration by increasing the local particle concentrations at the pressure nodes rapidly, with emphasis on those nodes in the bottom half of the domain.

4. Conclusion

A three-step numerical model solving the acoustic field and flow field by FDLBM, and tracking the particles by Lagrangian approach is developed. The numerical result matches with the experimental result. The simulation shows that the two non-linear acoustic effects—acoustic streaming and acoustic radiation pressure—encourage particle deposition. Acoustic streaming generates vortices and transports the particles to the wall, while acoustic radiation pressure forces the particles together and encourages agglomeration. Since the pressure drop by this setting is very low and the airflow velocity is not high, it

is potential to be developed into an energy-efficient filtration system. The developed model is a useful tool to optimize the design and for further investigating the problem.

Acknowledgements

The work was supported by the General Research Fund granted by the Research Grants Council of the Hong Kong Special Administrative Region, China (Project No. 611013).

References

[1] D. Thomas, P. Contal, V. Renaudin, P. Penicot, D. Leclerc, J. Vendel, Modelling pressure drop in HEPA filters during dynamic filtration, J. Aerosol Sci. 30 (2) (1999) 235–246.
[2] W.B. Faulkner, B.W. Shaw, Efficiency and pressure drop of cyclones across a range of inlet velocities, App. Eng. Agric. 22 (1) (2006) 155–161.
[3] C.M. Jang, D.W. Kim, S.Y. Lee, Performance characteristics of turbo blower in a refuse collecting system according to operation conditions, J. Mech. Sci. Technol. 22 (10) (2008) 1896–1901.
[4] W.T. Yuen, S.C. Fu, J.K.C. Kwan, C.Y.H. Chao, The use of nonlinear acoustics as an energy-efficient technique for aerosol removal, Aerosol Sci. Technol. 48 (9) (2014) 907–915.
[5] W.L. Nyborg, Acoustic streaming, Phys. Acoust. 2 (PtB) (1965) 265.
[6] J. Lighthill, Acoustic streaming, J. Sound Vib. 61 (3) (1978) 391–418.
[7] L.V. King, On the acoustic radiation pressure on spheres, Proc. R. Soc. Lond. Ser. A, Math. Phys. Sci. 147 (861) (1934) 212–240.
[8] L.P. Gorkov, On the forces acting on a small particle in an acoustical field and ideal fluid, Sov. Phys. Dokl. 6 (9) (1962) 773–775.
[9] J. Gallego-Juárez, E. Riera, G. RodrÍguez, T. Hoffmann, J. Gálvez, J. RodrÍguez, F. Gómez-Moreno, A. Bahillo-Ruiz, M. MartÍn-Espigares, M. Acha, Application of acoustic agglomeration to reduce fine particle emissions from coal combustion plants, Environ. Sci. Technol. 33 (21) (1999) 3843–3849.
[10] J.D. Sterling, S. Chen, Stability analysis of lattice Boltzmann methods, J. Comput. Phys. 123 (1996) 196–206.
[11] S. Chen, G.D. Doolen, Lattice Boltzamnn method for fluid flows, Annu. Rev. Fluid Mech. 30 (1998) 329–364.
[12] D.A. Wolf-Gladrow, Lattice-Gas Cellular Automata and Lattice Boltzmann Models: An Introduction, Springer-Verlag, Berlin, 2000, Chap. 5.
[13] S.C. Fu, W.W.F. Leung, R.M.C. So, A lattice Boltzmann method based numerical scheme for microchannel flows, J. Fluids Eng. 131 (2009) 081401.
[14] X. He, L.S. Luo, Lattice Boltzmann model for the incompressible Navier–Stokes equation, J. Stat. Phys. 88 (1997) 927–944.
[15] S.C. Fu, R.M.C. So, W.W.F. Leung, Stochastic finite difference lattice Boltzmann method for steady incompressible viscous flows, J. Comput. Phys. 229 (2010) 6084–6103.
[16] S.C. Fu, R.M.C. So, W.W.F. Leung, Linearized-Boltzmann-type-equation-based finite difference method for thermal incompressible flow, Comput. Fluids 69 (2012) 67–80.
[17] S.C. Fu, W.W.F. Leung, R.M.C. So, A lattice Boltzmann and immersed boundary scheme for model blood flow in constricted pipes: part 1 – steady flow, Commun. Comput. Phys. 14 (1) (2013) 126–152.
[18] G.H.R. Kefayati, FDLBM simulation of magnetic field effect on natural convection of non-Newtonian power-law fluids in a linearly heated cavity, Powder Technol. 256 (2014) 87–99.
[19] G.H.R. Kefayati, Mesoscopic simulation of double-diffusive mixed convection of Pseudoplastic fluids in an enclosure with sinusoidal boundary conditions, Comput. Fluids 97 (2014) 94–109.
[20] L. Rayleigh, On the circulation of air observed in Kundt's tubes, and on some allied acoustical problems, Philos. Trans. R. Soc. Lond. 175 (1884) 1–21.
[21] C.Y.H. Chao, M.P. Wan, A study of the dispersion of expiratory aerosols in unidirectional downward and ceiling-return type airflows using a multiphase approach, Indoor Air 16 (2006) 296–312.
[22] C.Y.H. Chao, M.P. Wan, G.N. Sze To, Transport and removal of expiratory droplets in hospital ward environment, Aerosol Sci. Technol. 42 (2008) 377–394.
[23] A. Li, G. Ahmadi, Dispersion and deposition of spherical particles from point sources in a turbulent channel flow, Aerosol Sci. Technol. 16 (1992) 209–226.
[24] P.D. Lax, Weak solutions of nonlinear hyperbolic equations and their numerical computation, Commun. Pure Appl. Math. 7 (1954) 159–193.
[25] F. Balboa Usabiaga, R. Delgado-Buscalioni, Minimal model for acoustic forces on Brownian particles, Phys. Rev. E 88 (2013) 063304.